Weierstraß-Institut
für Angewandte Analysis und Stochastik

im Forschungsverbund Berlin e.V.

Preprint ISSN 0946 – 8633

Stochastic simulation of flows and particle transport in porous tubes

K. Sabelfeld [1,3], O. Kurbanmuradov [2], and A. Levykin [3]

[1] Weierstrass Institute for Applied Analysis and Stochastics,
Mohrenstrase 39. D – 10117 Berlin, Germany;
E-Mail: sabelfel@wias-berlin.de

[2] Phys. Tech. Institute, Turkmenian University, Ashgabad
E-Mail: Kurbanmuradov@yandex.ru

[3] Institute of Computational Mathematics
and Mathematical Geophysics, Russian Acad. Sci.
Lavrentieva str.,6, 630090 Novosibirsk, Russia

No. 1324
Berlin 2008

1991 *Mathematics Subject Classification.* 65C05, 65C20, 76S05 .

Key words and phrases. Darcy equation, random hydraulic conductivity, Lagrangian trajectory, Randomized spectral models, lognormal random fields .

This work is supported partly by the RFBR Grant N 06-01-00498. O. Kurbanmuradov and A. Levykin acknowledge the host institute WIAS and the support of DAAD, under a 3 months Grant of 2007.

Edited by
Weierstraß-Institut für Angewandte Analysis und Stochastik (WIAS)
Mohrenstraße 39
10117 Berlin
Germany

Fax: + 49 30 2044975
E-Mail: preprint@wias-berlin.de
World Wide Web: http://www.wias-berlin.de/

Abstract

A Monte Carlo method is developed for stochastic simulation of flows and particle transport in tubes filled with a porous medium. The hydraulic conductivity is assumed to be a random field of a given statistical structure, the flow is modelled in a tube with prescribed boundary conditions. Numerical experiments are carried out by solving the random Darcy equation for each sample of the hydraulic conductivity by a SOR iteration method, and tracking Lagrangian trajectories in the simulated flow. We present and analyze different Eulerian and Lagrangian statistical characteristics of the flow such as transverse and longitudinal velocity correlation functions, diffusion coefficients, the mean and variance of Lagrangian trajectories, and discuss a "stagnation" effect which was found in our simulations.

1 Introduction

It is well known that the main difficulty in evaluation of pollutant transport in porous medium (e.g., in aquifers, filters, bio-materials, etc.) is the extreme heterogeneity of the media. This is a classical situation where there is a lack of knowledge about the local details of the spatial structure, but without this structure details, it is no chance to describe the large scale behavior. A natural approach is based on a stochastic description, where the heterogeneity are modeled as random fields with given statistical properties. In hydrology the stochastic approach is often used for the flow analysis in saturated zone (e.g., see [6], [26]). Stochastic approach allows to analyze also variations of other local properties, e.g., the chemical absorption coefficient [7,3], or the degradation constant [12].

In the flow simulation through a porous medium, one uses in the hydrology an Ansatz experimentally well supported that the hydraulic conductivity (in an alternative notations, the specific discharge) can be considered as a random field with a lognormal distribution. To analyze the Darcy equation with the random hydraulic conductivity in the case when its intensity of fluctuations is small, one applies the small perturbation method [21], [24]. We are aware of two versions of this method. The first version deals only with the variances, thus estimating only some deterministic scales of the process. The second version takes into account the spectral structure of the random solution, and thus it is able to construct samples of the random solutions and to evaluate practically arbitrary statistical characteristics of the solution. But since this approach works under the assumption of small fluctuation intensities, only a Gaussian approximation to the solution field is possible.

The case of large fluctuations is much more difficult, and can be treated by solving numerically the Darcy equation, say, by a finite difference or finite element methods, often called also stochastic finite element methods, e.g., see [9].

We develop in the present paper a direct stochastic simulation method for particle transport in a porous circular tube $D \subset I\!R^3$ of a finite length L and radius R. We assume that the axis of the tube coincides with the coordinate axis Ox. The hydraulic conductivity $K(\mathbf{x})$, $\mathbf{x} \in D$ is considered as a lognormal random field with a given correlation function.

Under the time independent flow condition and saturated porous media the so-called Darcy's velocity, or specific discharge, $\mathbf{q}$ is determined by the Darcy law:

$$\mathbf{q}(\mathbf{x}) = \theta(\mathbf{x})\mathbf{u}(\mathbf{x}) = -K(\mathbf{x})\nabla(\phi(\mathbf{x})) \tag{1}$$

where $\mathbf{u}$ is the pore velocity, θ, the porosity, ϕ, the hydraulic potential $\phi = z + p/(g\rho)$, ρ, the fluid density, and K is the hydraulic conductivity.The functions θ and K are the key parameters of the flow. Experimental measurements show high heterogeneous behavior of K in space with the following remarkable property: when considering K as a random field, its distribution is well approximated by the log-normal law (e.g., see [2], [8]). Therefore, in models, the hydraulic log conductivity $Y = \ln K$ is commonly considered as a statistically homogeneous random field . Let $Y' = Y - \langle Y \rangle$, and let $B_Y(\mathbf{r}) = \langle Y'(\mathbf{x}+\mathbf{r})Y'(\mathbf{x})\rangle$ be the correlation function of the hydraulic log conductivity. Here and throughout the paper the angle brackets stand for the expectation over the relevant distribution of the random field Y.

The porosity θ is also often considered in some models as a random field. However its variability is generally much smaller than that of K and it is usually assumed to be constant.

Let us denote by $c(\mathbf{x}, t)$ the concentration of a passive scalar transported by the flow $\mathbf{u}(\mathbf{x})$ in the tube. This process is governed by the convection-diffusion equation

$$\frac{\partial c(\mathbf{x}, t)}{\partial t} + \mathbf{u}(\mathbf{x}) \cdot \nabla c = -\beta c(\mathbf{x}, t) + D_l \Delta c + f(\mathbf{x}, t), \tag{2}$$

where β is an absorption coefficient, D_l is a local (pore-scale) diffusion coefficient, $f(\mathbf{x}, t)$ is the distribution density function of the particle sources. In the case when R, the radius of the tube is considerably less than its length L, then after a certain transitional time, the dynamics of the mean concentration $C = \langle c \rangle$ can be described by the one-dimensional convection-diffusion equation

$$\frac{\partial C(x,t)}{\partial t} + U\frac{\partial C(x,t)}{\partial x} = -\beta C(x,t) + D_m \frac{\partial^2 C(x,t)}{\partial x^2} + Q(x,t), \tag{3}$$

where x is the longitudinal coordinate, Q is an integral source defined as an integral of the density f over the cross-section of the tube, U is the mean longitudinal Lagrangian velocity, D_m is the longitudinal diffusion coefficient.

The main difficulty in the presented method is that the coefficients U and D_m in the up-scaled equation of convection-diffusion depend on the statistical structure of the random velocity $\mathbf{u}(\mathbf{x})$, the coefficient of local diffusion D_l, and on the radius of the tube R. Even in the case when the log conductivity $Y(\mathbf{x}) = \ln K(\mathbf{x})$ is a homogeneous Gaussian random field, the statistical structure of the velocity field is defined by the mean $< Y >$, variance σ_Y^2, the correlation length scale l_Y, and the mean longitudinal velocity along the tube's axis, U_0. It means that even if $Y(\mathbf{x})$ is an isotropic random field, the quantities U and D_m are functions of a series of parameters, namely, $< Y >$, σ_Y, l_Y, U_0, D_l, R:

$$U,\, D_m = \mathcal{F}(< Y >, \sigma_Y, l_Y, U_0, D_l, R). \tag{4}$$

In this paper we will use this type of dependence to establish properties of the form (4) for the Gaussian correlation function (see below (11)). In practice, the exponential correlations (12) are also often used.

2 Problem setting

Let us consider a flow in a circular porous tube

$$D = \{\mathbf{x} \in I\!R^3 \,:\, x = x_1 \in [0, L],\, \rho^2 = x_2^2 + x_3^2 \le R^2\}\ ,$$

where L and R are the length and the radius, respectively.

We will assume that the porosity is constant, so the flow is divergenceless

$$\nabla \cdot \mathbf{u}(\mathbf{x}) = \nabla \cdot (K(\mathbf{x})\nabla\phi(\mathbf{x})) = 0. \tag{5}$$

Concerning the boundary conditions, we assume impermeable boundary conditions on the wall of the tube, i.e.,

$$\frac{\partial\phi}{\partial\mathbf{n}_\mathbf{x}} = 0,\ \mathbf{x} \in \Gamma = \{\mathbf{x} \in I\!R^3 : x = x_1 \in [0, L],\ \rho^2 = x_2^2 + x_3^2 = R^2\}, \tag{6}$$

where $\mathbf{n}_\mathbf{x}$ is the outer unit normal vector to Γ at the point $\mathbf{x} \in \Gamma$. On the tube's inlet and outlet, the boundary conditions are taken as follows:

$$\phi(0, x_2, x_3) = 0, \quad \phi(L, x_2, x_3) = -JL, \quad x_2^2 + x_3^2 \le R^2, \tag{7}$$

where $J > 0$ is a dimensionless constant which we fix as $J = 1$.

The particle concentration $c(\mathbf{x}, t)$ is to be found from (2) with the following boundary conditions: on the wall we prescribe no concentration flux:

$$\mathbf{q}(\mathbf{x}, t) \cdot \mathbf{n}_\mathbf{x} = 0,\ \mathbf{x} \in \Gamma, \tag{8}$$

and on the tube's ends we prescribe

$$q_1(0, x_2, x_3, t) = q_0(x_2, x_3), \quad c(L, x_2, x_3, t) = 0, \quad x_2^2 + x_3^2 \le R^2, \tag{9}$$

where the column-vector $\mathbf{q}(\mathbf{x}, t) = (q_1(\mathbf{x}, t), q_2(\mathbf{x}, t), q_3(\mathbf{x}, t))^T$ is the flux defined by

$$\mathbf{q}(\mathbf{x}, t) = \mathbf{u}(\mathbf{x})c(\mathbf{x}, t) - D_l\nabla c(\mathbf{x}, t) = -\frac{K(\mathbf{x})}{\theta}\nabla\phi(\mathbf{x}) - D_l\nabla c(\mathbf{x})\ ,$$

$q_0(x_2, x_3)$ is the source distribution. We take $f(\mathbf{x}) = 0$ in the right-hand side of (2), and the same for the initial concentration:

$$C(\mathbf{x}, 0) = 0, \quad \mathbf{x} \in D. \tag{10}$$

Thus the concentration field $C(\mathbf{x}, t)$ is defined from (5)-(10). Note that the hydraulic conductivity $K(\mathbf{x})$ is assumed to be a random field, so the concentration $c(\mathbf{x}, t)$ is also a random field. Its simplest statistical characteristics is the mean $C(\mathbf{x}, t) = \langle c(\mathbf{x}, t)\rangle$ which is of high practical interest. Important in applications are also the fluctuation intensity defined as the ratio of r.m.s. of the concentration to the mean concentration, and the probability that the concentration exceeds a given critical level. These statistical characteristics depend on the statistical characteristics of the porous medium, i.e., the log conductivity $\langle Y\rangle$, its variance $\sigma_Y^2 = \langle Y'^2\rangle$ and correlation function $B_Y(\cdot)$, as well as on the length and radius of the tube, the pressure flux J, and the coefficients of absorption and diffusion β and D_l.

Note that the analysis of the dependence even of the simplest statistical characteristics, the mean concentration, on the set of all parameters we listed above is very difficult, so it is reasonable to make some additional assumptions.

Here we will assume that the log conductivity $\ln K(\mathbf{x})$ has an axial symmetry, hence, it depends only on two coordinates, $x = x_1$ and $\rho = \sqrt{x_2^2 + x_3^2}$. We assume additionally that $\ln K(\mathbf{x}) = Y(\mathbf{x}) = \langle \ln K\rangle + \mathcal{Y}'(x, \rho)$, where $\mathcal{Y}'(x, \rho)$ is a homogeneous Gaussian random field with zero mean which depends on $(x, \rho) \in I\!R^2$.

Two typical variants of correlation function $B_{\mathcal{Y}}(x,\rho) = \langle \mathcal{Y}'(x+x',\rho+\rho')\mathcal{Y}'(x',\rho')\rangle$ are: *Gaussian correlation function*

$$B_{\mathcal{Y}}(x,\rho) = \sigma_Y^2 \exp\Big\{ -\frac{x^2}{l_x^2} - \frac{\rho^2}{l_\rho^2}\Big\} \tag{11}$$

and *Exponential correlation function*

$$B_{\mathcal{Y}}(x,\rho) = \sigma_Y^2 \exp\Big\{ -\big(\frac{x^2}{l_x^2} + \frac{\rho^2}{l_\rho^2}\big)^{1/2}\Big\} \ . \tag{12}$$

Thus, even for constant q_0, in our model the mean concentration $C(x,\rho,t)$ is a function of three variables, with 11 input parameters θ, $\langle Y\rangle$, σ_Y, l_x, l_ρ, L, R, J, β, D_l, q_0. Without loss of generality we put $\theta = 1$ and $q_0 = 1$.

3 Finite-difference approximation

In cylindrical coordinates (ρ,ψ,x), the equation (5) takes the form

$$\frac{1}{\rho}\frac{\partial}{\partial\rho}(\rho K\frac{\partial\phi}{\partial\rho}) + \frac{1}{\rho^2}\frac{\partial}{\partial\psi}(K\frac{\partial\phi}{\partial\psi}) + \frac{\partial}{\partial x}(K\frac{\partial\phi}{\partial x}) = 0. \tag{13}$$

It is assumed that the functions K and ϕ do not depend on the angle ψ, so the potential $\phi(x,\rho)$ is to be found from the equation

$$\frac{1}{\rho}\frac{\partial}{\partial\rho}(\rho K\frac{\partial\phi}{\partial\rho}) + \frac{\partial}{\partial x}(K\frac{\partial\phi}{\partial x}) = 0 \tag{14}$$

with the following boundary conditions

$$\frac{\partial\phi}{\partial\rho} = 0, \quad \rho = R, \tag{15}$$

$$\lim_{\rho\to 0}\frac{\partial\phi}{\partial\rho} = 0 \ , \tag{16}$$

and

$$\phi(0,\rho) = 0, \quad \phi(L,\rho) = -L, \quad 0 \le \rho \le R. \tag{17}$$

A finite-difference approximation of (14) for the inner nodes of the mesh

$$\rho_i = \rho_{i-1} + h_1,\ i = 1,\dots,N_1,\ \rho_0 = 0,\ h_1 = R/N_1$$

$$x_i = x_{i-1} + h_2,\ i = 1,\dots,N_2,\ x_0 = 0,\ h_2 = L/N_2$$

was chosen as follows:

$$\frac{1}{\rho_i h_1}(\rho_{i+\frac12}K_{i+\frac12,j}\frac{\phi_{i+1,j}-\phi_{i,j}}{h_1} - \rho_{i-\frac12}K_{i-\frac12,j}\frac{\phi_{i,j}-\phi_{i-1,j}}{h_1}) + \frac{1}{h_2}(K_{i,j+\frac12}\frac{\phi_{i,j+1}-\phi_{i,j}}{h_2} - K_{i,j-\frac12}\frac{\phi_{i,j}-\phi_{i,j-1}}{h_2}) = 0 \ . \tag{18}$$

The boundary conditions (15)-(16) were approximated by

$$-\frac{(2L-h_1)K_{N_1-\frac12,j}}{Lh_1^2}(\phi_{N_1,j}-\phi_{N_1-1,j}) + (K_{N_1,j+\frac12}\frac{\phi_{N_1,j+1}-\phi_{N_1,j}}{{h_2}^2} - K_{N_1,j-\frac12}\frac{\phi_{N_1,j}-\phi_{N_1,j-1}}{{h_2}^2}) = 0, \tag{19}$$

$$\frac{2K_{\frac{1}{2},j}(\phi_{1,j}-\phi_{0,j})}{{h_1}^2}+\frac{1}{h_2}(K_{0,j+\frac{1}{2}}\frac{\phi_{0,j+1}-\phi_{0,j}}{h_2}-K_{0,j-\frac{1}{2}}\frac{\phi_{0,j}-\phi_{0,j-1}}{h_2})=0, \tag{20}$$

and at the ends of the tube the Dirichlet condition (17) was approximated by $\phi_{i,0}=0,\ \phi_{i,N_2}=-L,\ i=0,1,\ldots,N_1$.

The presented finite-difference relations (18)-(20) approximate the original problem (14)-(17) with the second order (e.g., see [23]). In matrix notation, the system (18)-(20) can be written as follows:

$$A\bar{\phi}=(Diag(A)-L-U)\bar{\phi}=f \tag{21}$$

where $Diag(A)$ is the diagonal matrix with the diagonal entries $\{a_{ii}\}$, L and U are the left and right triangular matrices: $L=\{-a_{ij}\}_{j>i}$, $U=\{-a_{ij}\}_{j<i}$. The entries a_{ij} are defined by the linear relations (18)-(20) and the ordering of the nodes. We have used the following ordering: the entries a_{ij}, $i=0,2\ldots,N_1$, $j=1,2\ldots,N_2-1$ are defined so that the fixed i corresponds to a fixed value of ρ, while the increase of j means we move along x (from right to left) when i is fixed. The lower bound of domain corresponds to $i=0$, the upper bound has the index $i=N_1$, while the right end corresponds to $j=0$, and the left end of the tube is indexed by N_2. The solution column-vector $\bar{\phi}$ has the form

$$\bar{\phi}=(\phi_{0,1},\ldots,\phi_{0,N_2-1},\,\phi_{11},\ldots,\phi_{1,N_2-1},\,\ldots,\phi_{N_1,1},\ldots,\phi_{N_1,N_2-1})^T\ .$$

The right hand side of our system (21) f is a vector of the same structure whose entries all equal zero excluding the last entries corresponding to the boundary conditions, i.e., f_{0,N_2-1}, $f_{1,N_2-1},\ \ldots$ and f_{N_1,N_2-1} are the non-zero entries which can be easily obtained from the boundary conditions (18) and (20) .

To solve the system (21), we apply the successive over relaxation (SOR) method with an adaptive choice of the parameter ω_n:

$$\bar{\phi}_n=\omega_n[Diag(A)]^{-1}(f+L\bar{\phi}_n+U\bar{\phi}_{n-1})+(1-\omega_n)\bar{\phi}_{n-1}\ .$$

Note that the matrix A is symmetric and positive definite which guaranties the convergence of the SOR method under some additional restrictions on the parameter ω_n (e.g., see [33]). The iterations were made until the error satisfies $\varepsilon=\|\ \bar{\phi}-\bar{\phi}_n\ \|\leq 10^{-6}$. The mesh size h was chosen dependent on the fluctuation intensity as follows: $h=cl/5,\ cl/10,\ cl/20$ for $\sigma=0.5,\ 1.0,\ 2.0$, respectively. Here cl is the correlation length which in our case was fixed as $cl=1$.

4 Statistical characteristics of the flow

It is convenient to choose dimensionless variables

$$\tilde{\mathbf{x}}=\frac{\mathbf{x}}{\lambda},\quad \tilde{\mathbf{u}}=\frac{\theta\mathbf{u}}{K_GJ},\quad \tilde{\phi}=\frac{\phi}{J\lambda},$$

where $K_G=e^{\langle Y\rangle}$, λ is a characteristic length scale. Since the velocity does not depend on the polar angle in our cylindrical coordinate system (recall that the axis of the tube is coincident with the x_1-coordinate) we get

$$\mathbf{u}(\mathbf{x})=\frac{K_GJ}{\theta}\tilde{\mathbf{u}}(x/\lambda,\rho/\lambda). \tag{22}$$

Here $\tilde{\mathbf{u}}(\tilde{\mathbf{x}})$ is a dimensionless function which solves the problem (5)-(7) where the variable $\mathbf{x}$ should be changed with $\tilde{\mathbf{x}}$, then put $J=1$, change L and R with the dimensionless variables

$\tilde{L} = L/\lambda$ and $\tilde{R} = R/\lambda$; in addition, the log conductivity field Y should be taken so that $\langle Y \rangle = 0$ with the correlation function (11) or (12) where the dimensional scales l_x and l_ρ should be changed with dimensionless scales $\tilde{l_x} = l_x/\lambda$ and $\tilde{l_\rho} = l_\rho/\lambda$, respectively.

Thus the dimensionless velocity $\tilde{\mathbf{u}}(\tilde{\mathbf{x}})$ depends not only on the main variable $\tilde{\mathbf{x}}$ but also on 5 dimensionless parameters σ_Y, $\tilde{l_x}$, $\tilde{l_\rho}$, $\tilde{L}$, $\tilde{R}$.

Remark 1. If we take for λ one of the parameters L, R, l_x or l_ρ, we can reduce the number of parameters to 4. We take further $\lambda = l_x$. In what follows we use dimensionless variables, so it is not necessary to use the sign $\tilde{\cdot}$.

4.1 Eulerian statistical characteristics of the velocity field

So let us consider a velocity field $\mathbf{u}(\mathbf{x}) = (u_x(\mathbf{x}), u_y(\mathbf{x}), u_z(\mathbf{x}))^T$ in the cylindrical coordinate system (x, ρ, ϕ) where the tube's axis coincides with the direction Ox_1: $x = x_1$, $\rho = (x_2^2 + x_3^2)^{1/2}$. We denote by u_ρ the transverse (radial) velocity component $u_\rho(\mathbf{x}) = e^{Y(\mathbf{x})} \cdot \frac{\partial \phi(\mathbf{x})}{\partial \rho}$. Under the assumptions made, the longitudinal and transverse velocities u_x and u_ρ in this cylindrical coordinate system (x, ρ, ϕ) depend only on the variables (x, ρ) and satisfy the incompressibility condition:

$$\frac{\partial}{\partial x}(\rho u_x(x, \rho)) + \frac{\partial}{\partial \rho}(\rho u_\rho(x, \rho)) = 0. \tag{23}$$

4.1.1 One-point statistical characteristics of the velocity field

If L is much larger than 1, then in the inner region (i.e., x belongs to a core region, sufficiently far from the ends of the tube) the statistical characteristics of $\mathbf{u}$ depend on the anisotropy parameter $\kappa = l_\rho/l_x$, radius R and on the variance of log conductivity σ_Y. We have now to estimate quantitatively this inner region.

We assume that the log conductivity Y is a Gaussian random field with the Gaussian correlation function (11), and $\kappa = 1$ (this means, Y is isotropic).

We take $L = 100$, $R = 20$, and $\sigma_Y = 1$.

In Figure 1 we show the mean longitudinal velocity $\langle u_x \rangle$ (left panel) and its mean square deviation σ_u (right panel), as functions of ρ, for different values of σ_Y. The value of the longitudinal coordinate was here fixed so that $x/l_x = 5$ where l_x is the correlation length.

Figure 2 presents the same curves for different values of x/l_x. From this figure it is clearly seen that the functions tend to a steady state after $x > 2$, that is, these curves are becoming practically independent of the longitudinal coordinate.

An important property of the flow is that the longitudinal velocity integrated over the cross-section of the tube, $U_x = 2\pi \int_0^R u_x(x, \rho)\, \rho d\rho$, should be constant. This follows from the continuity equation (23), and the boundary condition on the side surface of the tube. The value of this constant depends on the parameters R, L, σ_Y. It may also vary from one sample to another. However due to the errors of the finite-difference method the numerically constructed samples of the function $U_x(x)$ can be slightly biased away from the constant value. In Figure 3 (left panel) we show for illustration two samples of this function (thin and thick curves), for two values of the grid size h of the finite-difference approximation to (5). Here and in what follows, we denote by n_0 the number of harmonics in the spectral representation we used for modeling

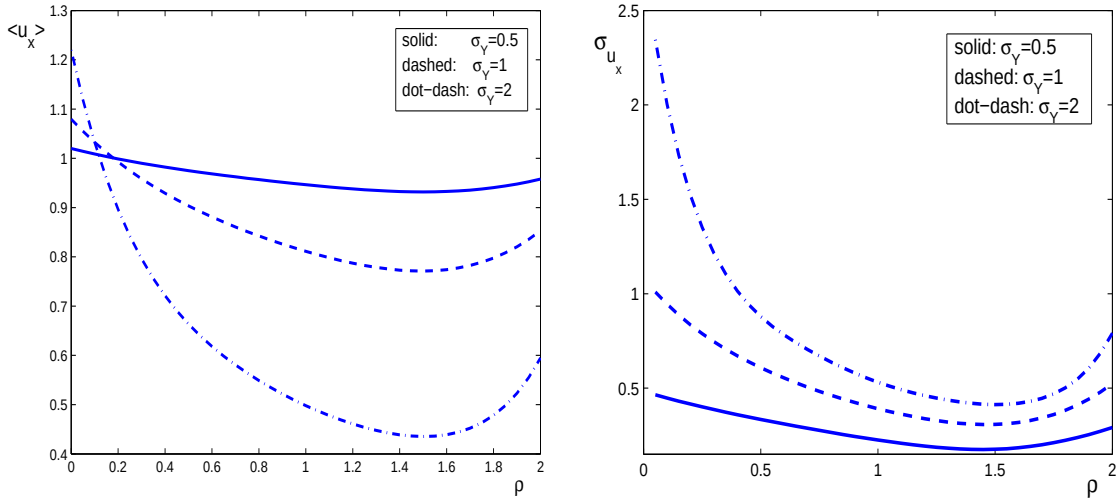

Figure 1: The mean longitudinal velocity component (left panel), and its mean square deviation σ_u (right panel) versus the transverse coordinate ρ, for three values of the variance σ_Y. The tube's length was $L = 20$, the radius $R = 2$.

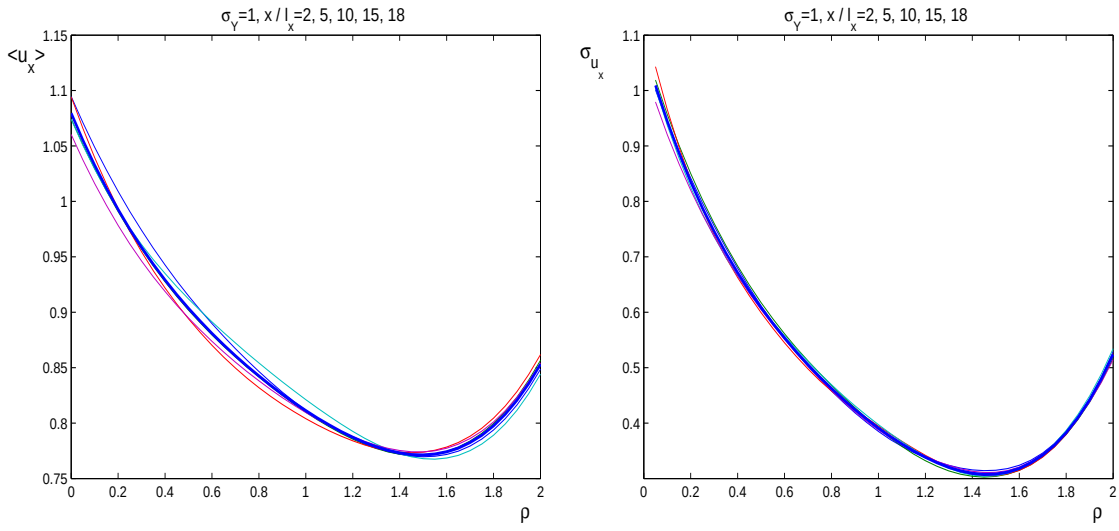

Figure 2: The mean longitudinal velocity component (left panel), and its variance (right panel) versus the transverse coordinate ρ, for five different values of x/l_x, and $\sigma_Y = 1$.The tube's length was $L = 20$, the radius $R = 2$.

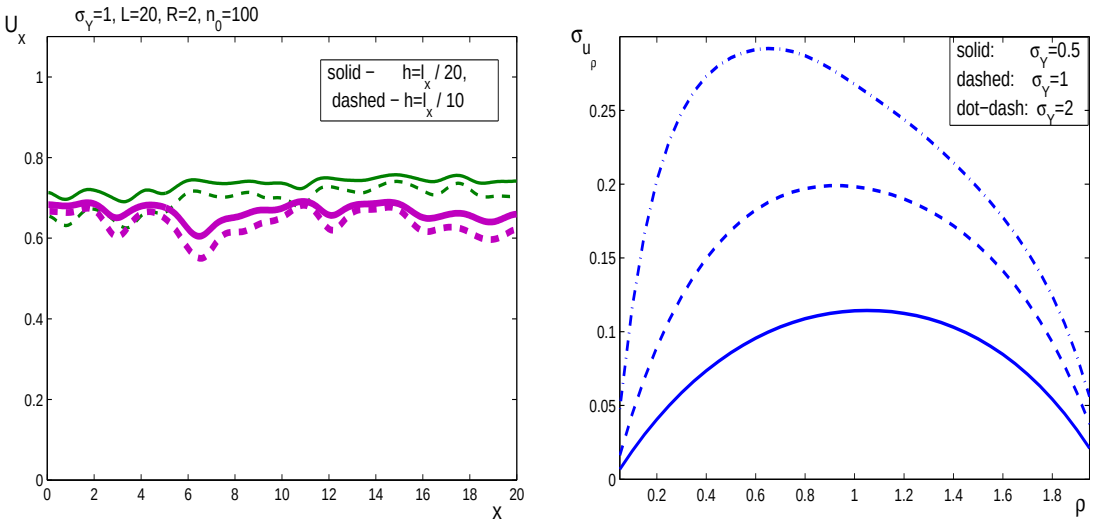

Figure 3: Left panel: two samples of the cross-averaged longitudinal velocity U_x as a function of x, for two different values of the integration step $h = 0.1$ (dashed) and $h = 0.05$ (solid). Right panel: the standard deviation of the transversal velocity u_ρ versus the transverse coordinate ρ, for three values of the variance σ_Y; The radius and the length of the tube are the same as in Figures 1 and 2.

the log conductivity Y. The calculations confirm the theoretical considerations that the error (the deviation of U_x from the constant value) decreases with the decrease of h. The relative error is approximately 5% for $h = 0.05$. Throughout the paper we use this grid with $h = 0.05$ in all our calculations except for some cases we will additionally mention.

As to the mean transverse velocity u_ρ, we get from the continuity equation (23)

$$\frac{\partial}{\partial x}(\rho\langle u_x(x,\rho)\rangle) + \frac{\partial}{\partial \rho}(\rho\langle u_\rho(x,\rho)\rangle) = 0. \tag{24}$$

Far from both ends of the tube the mean $\langle u_x(x,\rho)\rangle$ does not depend on x, hence from (24) it follows that $\rho\langle u_\rho(x,\rho)\rangle = Const$. From this, using the impermeability conditions $u_\rho(x,R) = 0$ we conclude that the constant in the right-hand side of the last equality vanishes, i.e., $\langle u_\rho(x,\rho)\rangle = 0$ for all $\rho \in [0,R]$. Our calculations confirm this conclusion.

The mean square deviation of the transversal velocity u_ρ is an important characteristic. We plot it in Figure 3 (right panel) as a function of ρ; the value of x was the same as in Figure 1.

4.1.2 Correlation functions

Let $u'_x = u_x - \langle u_x\rangle$, $u'_\rho = u_\rho - \langle u_\rho\rangle$. We deal with the following main correlation functions

$$B_{xx}(x,x';\rho) = \langle u'_x(x+x',\rho)u'_x(x',\rho)\rangle, \quad B_{\rho\rho}(x,x';\rho) = \langle u'_\rho(x+x',\rho)u'_\rho(x',\rho)\rangle,$$

which are correlations along the longitudinal coordinate, and

$$B_{x\rho}(x,x';\rho) = \langle u'_x(x+x',\rho)u'_\rho(x',\rho)\rangle$$

is the cross-correlation of the velocities u_x and u_ρ.

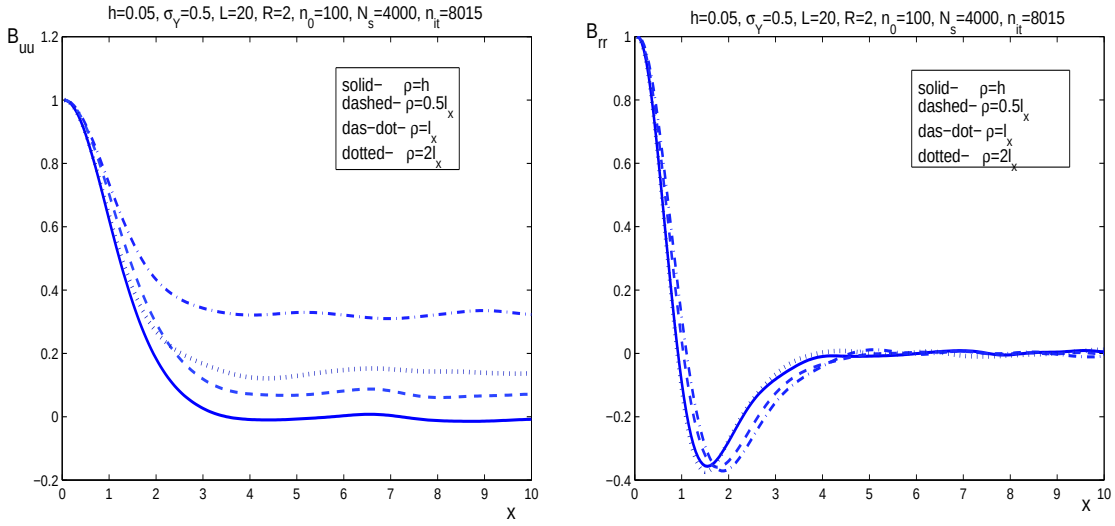

Figure 4: The normalized correlation function of the longitudinal (left panel) and transversal (right panel) velocities versus the longitudinal coordinate, for 4 different fixed values of ρ; $\sigma_Y = 0.5$.

We can expect that inside the tube, when we are far enough from both tube's ends, these correlations will be almost independent of x', hence, they can be considered as functions of two variables (x, ρ). This implies that in this inner region, the velocity $(u_x(x,\rho), u_\rho(x,\rho))$ is almost stationary with respect to the longitudinal coordinate x. As our calculations show, this inner region can be defined as a domain where x and x' are not closer to the both tube's ends than about two correlation lengths. Thus in this inner region we have an approximate homogeneity in the longitudinal direction, and the functions $B_{xx}(x, x'; \rho)$, $B_{\rho\rho}(x, x'; \rho)$ depend on the distance $X = x' - x$ only.

In Figures 4-6 we present the normalized correlations $B_{uu}(X;\rho) = B_{xx}(x, x+X; \rho)/B_{xx}(x, x, \rho)$, $B_{rr}(X;\rho) = B_{\rho\rho}(x, x+X; \rho)/B_{\rho\rho}(x, x; \rho)$, at $x = 5$, for four different values of ρ and three different values of σ. The number of samples here and in almost all calculations throughout the paper (if otherwise not mentioned) was taken as $N_s = 4000$.

It is interesting to note that the normalized correlation of the longitudinal velocity, $B_{uu}(X;\rho)$ tends to a non-zero asymptotic in a core region, i.e., far both from the side surface, and the axis. This can be seen for instance in Figures 4-6, see the dash-dot curve which corresponds to $\rho = 1$. This can be explained by a symmetric influence of the side surface of the tube.

Note that as the tube's length is increased, the asymptotical values for $B_{uu}(X;\rho)$ are decreased. This can be clearly seen in Figure 7 (left panel) where we present the results for the tube's length $L = 50$. But there is almost no change in the asymptotical values of $B_{rr}(X;\rho)$, see the curves in the right panel of Figure 7.

As we mentioned above, the velocity U_x (defined as an average over the tube's cross-section), which is of course random, should be independent of the longitudinal coordinate. In what follows we call U_x for brevity as cross-averaged velocity. This random velocity has a clear physical meaning, it just characterizes the random longitudinal velocity of a total mass of a cloud of particles initially uniformly distributed over the tube's cross-section. The concentration of the particles is then governed by a $1D$ convection-diffusion equation (3) where the convective term $U =< U_x >$.

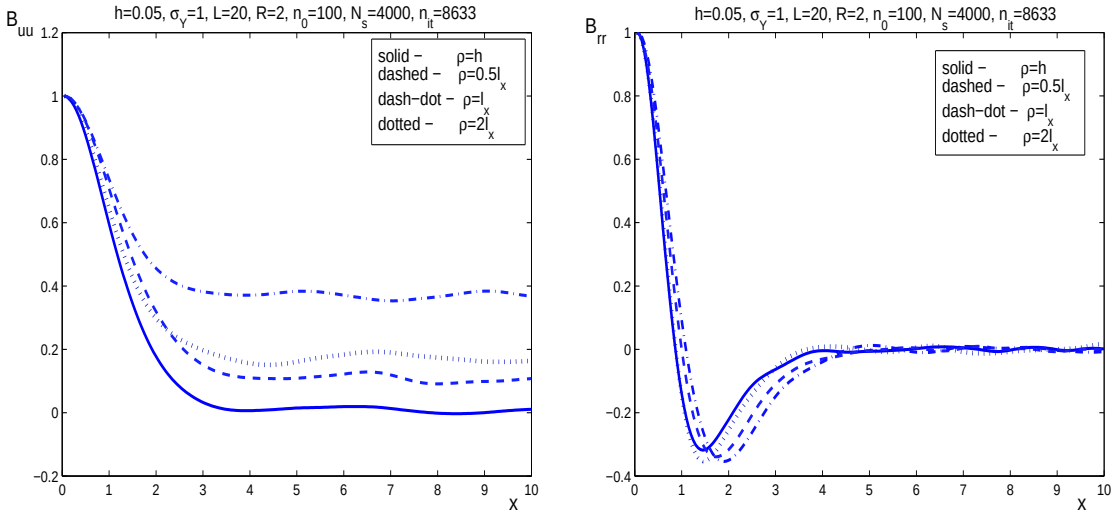

Figure 5: The same as in Figure 4, but for $\sigma_Y = 1$.

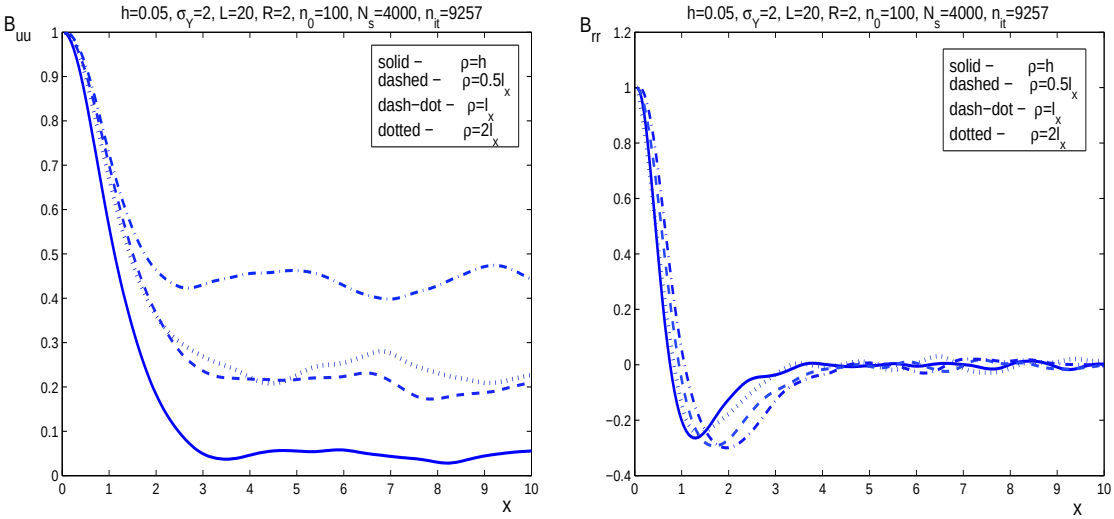

Figure 6: The same as in Figure 4, but for $\sigma_Y = 2$.

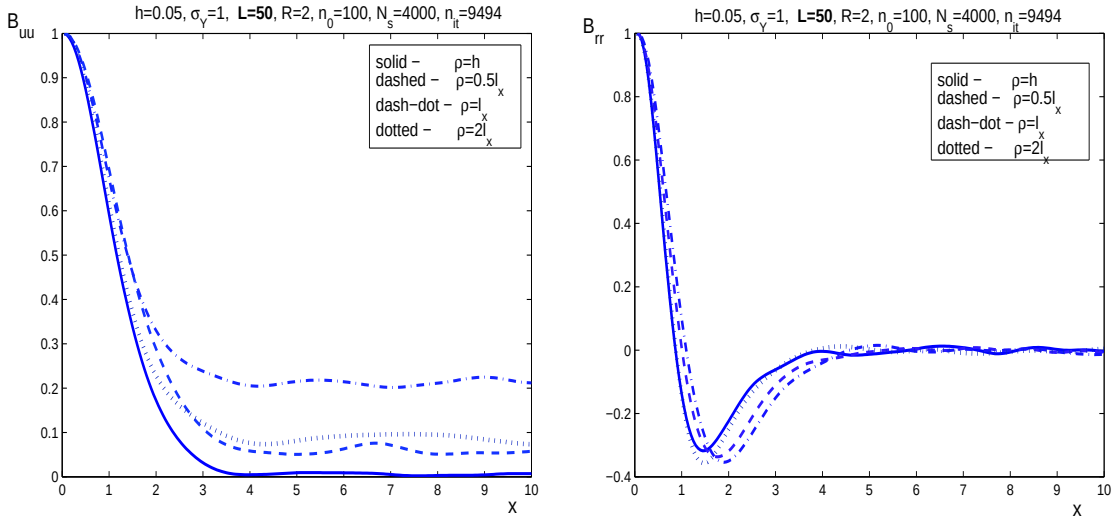

Figure 7: The same as in Figure 5, but for $L = 50$.

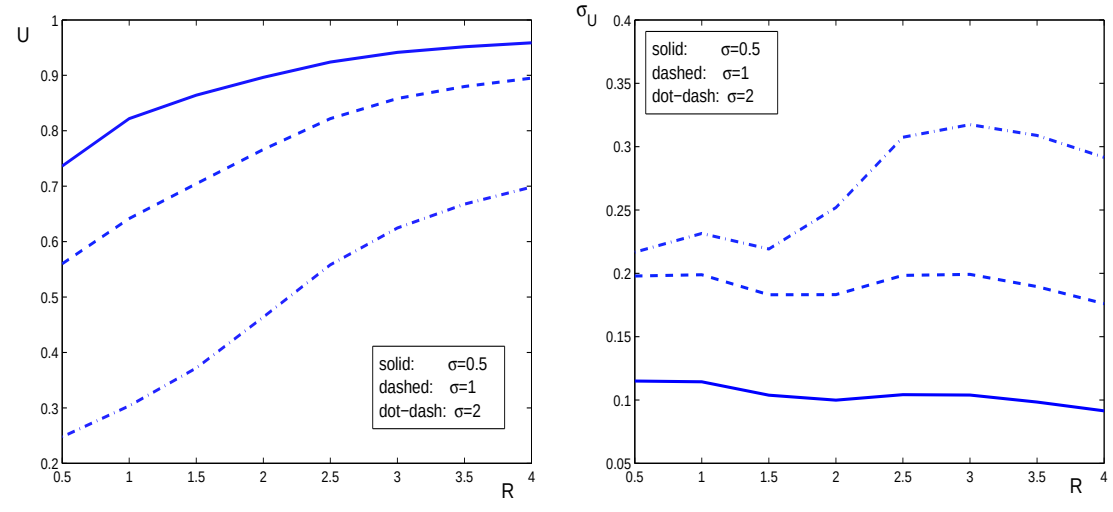

Figure 8: The mean of the cross-averaged longitudinal velocity (left panel) ant its standard deviation (right panel) versus the radius of the tube R, for three different values of σ_Y. The tube's length was $L = 50$.

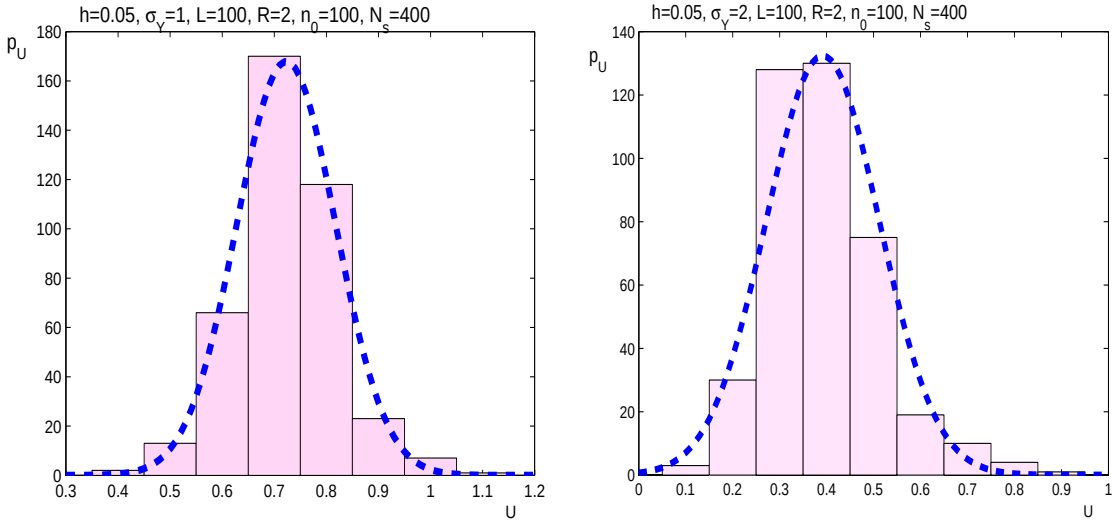

Figure 9: The histograms of the cross-averaged longitudinal velocity, for two values of σ_Y: $\sigma_Y = 1$ (left panel), and $\sigma_Y = 2$ (right panel). The tube's length is $L = 100$.

In Figure 8 we present U, the ensemble mean of the cross-averaged velocity U_x (left panel) and its standard deviation $\sigma_U = (\langle U_x^2 \rangle - \langle U_x \rangle^2)^{1/2}$ (right panel) versus the tube's radius, for the fixed length $L = 50$. Different curves correspond to different values of σ_Y. These results show that the dependence of U and σ_U on the tube's radius is larger for larger values of σ_Y. This dependence can be useful when solving inverse problems of determining the porous medium characteristics (in our case, the parameters of the hydraulic conductivity) through measurement of the flow.

In Figures 9-10 we show the histograms of the pdf $p_U(U) = \langle \delta(U - U_x) \rangle$, for different values of σ_Y and L. Here we had $N_s = 400$ samples for the case $L = 100$, and $N_s = 4000$ for $L = 20$. To see the deviation from the Gaussian distribution, we show for comparison the Gaussian pdf with the same mean and variance. From these results (see Figure 9) it is seen that the pdf becomes closer to a Gaussian pdf as the tube's length increases. For smaller radii (see Figure 10) the pdf is quite asymmetric.

4.2 Lagrangian statistical characteristics of the velocity field

The Lagrangian statistical characteristics are the most important functions in the analysis of the particle transport. In particular, often used is the mean Lagrangian velocity of a particle, and the diffusivity.

Let us define these statistical characteristics. We denote by $\mathbf{x}_0$ the starting coordinate of a fluid particle whose Lagrangian trajectory is $\mathbf{X}(t;\mathbf{x}_0) = (X(t;\mathbf{x}_0), Y(t;\mathbf{x}_0), Z(t;\mathbf{x}_0))$, $t \geq 0$, and $\mathbf{V}(t;\mathbf{x}_0) = \mathbf{u}(\mathbf{X}(t;\mathbf{x}_0))$ is the Lagrangian velocity. By definition, $\mathbf{X}(t;\mathbf{x}_0)$ is a solution of the following problem

$$\frac{d\mathbf{X}}{dt} = \mathbf{u}(\mathbf{X}),\ t > 0; \quad \mathbf{X}(0) = \mathbf{x}_0. \tag{25}$$

The behavior of the trajectory near the boundary of the tube should be arranged in accordance with the boundary conditions imposed for the flow. Since we have chosen the impenetrable conditions on the side surface of the tube, the Lagrangian trajectory never reaches the boundary.

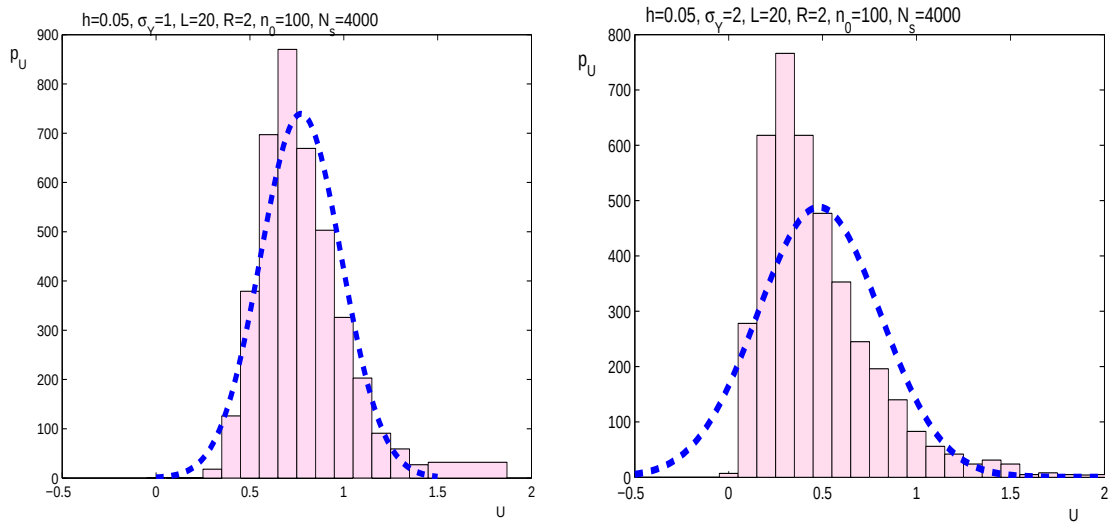

Figure 10: The same as in Figure 9, but for $L = 20$.

The particle stops when it reaches the left end ($x = 0$), or the right end ($x = L$) of the tube. In the cylindrical coordinate system, $X(t;\mathbf{x}_0)$, $\mathcal{R}(t;\mathbf{x}_0) = (Y(t;\mathbf{x}_0) + Z(t;\mathbf{x}_0))^{1/2}$), using the notation for the velocities as , $V_x(t;\mathbf{x}_0) = u_x(X(t;\mathbf{x}_0), \mathcal{R}(t;\mathbf{x}_0))$, $V_r(t;\mathbf{x}_0) = u_\rho(X(t;\mathbf{x}_0), \mathcal{R}(t;\mathbf{x}_0))$ we write the motion equation of a particle starting at (x_0, ρ_0) as follows

$$\frac{dX}{dt} = u_x(X(t), \mathcal{R}(t)),\ \frac{d\mathcal{R}}{dt} = u_\rho(X(t), \mathcal{R}(t)),\ t > 0\ ,$$
$$X(0) = x_0, \quad \mathcal{R}(0) = \rho_0\ . \tag{26}$$

The Lagrangian processes $(X(t;\mathbf{x}_0),\ \mathcal{R}(t;\mathbf{x}_0))$ and $(V_x(t;\mathbf{x}_0),\ V_\rho(t;\mathbf{x}_0))$ depend on the starting point $\mathbf{x}_0$, i.e., on $(x_0,\ \rho_0)$, so to show this, we use the notation $(X(t;x_0,\ \rho_0),\ \mathcal{R}(t;x_0,\ \rho_0;))$ and $(V_x(t;x_0,\ \rho_0),\ V_r(t;x_0,\ \rho_0;))$ for these Lagrangian trajectories.

Now we define the main Lagrangian statistical characteristics we deal with in this paper. Let $(x_0,\ \rho_0)$ be the starting point of a Lagrangian trajectory. The mean of the longitudinal coordinate is $\bar{X}(t;x_0,\ \rho_0) = \langle X(t;x_0,\ \rho_0)\rangle$, and $D_X(t;x_0,\ \rho_0) = \langle (X'(t;x_0,\ \rho_0))^2\rangle$ is its variance. Analogously, we define the mean transverse coordinate $\langle\mathcal{R}(t)\rangle$ and its variance $\sigma^2_{\mathcal{R}}(t) = \langle\mathcal{R}^2(t)\rangle - \langle\mathcal{R}(t)\rangle^2$.

The Lagrangian correlation functions of the longitudinal and transverse velocities are denoted by $\langle V'_x(t;x_0,\rho_0)V'_x(0;x_0,\rho_0)\rangle$, and $\langle V'_r(t;x_0,\rho_0)V'_r(0;x_0,\rho_0)\rangle$, respectively. The mean longitudinal velocity is $\langle V_x(t;x_0,\ \rho_0)\rangle$, and the variances of the longitudinal and transversal velocities are $\langle (V'_x(t;x_0,\ \rho_0))^2\rangle$ and $\langle (V'_r(t;x_0,\ \rho_0))^2\rangle$, respectively.

The diffusion coefficients are defined by

$$K_x(t;x_0,\ \rho_0) = \langle X'_x(t;x_0,\ \rho_0)V'_x(t;x_0,\ \rho_0)\rangle\ ,$$
$$K_r(t;x_0,\ \rho_0) = \langle \mathcal{R}'_x(t;x_0,\ \rho_0)V'_r(t;x_0,\ \rho_0)\rangle\ .$$

Here $X' = X - \langle X\rangle, V' = V - \langle V\rangle$.

In Figure 11 we present the mean of the transverse coordinate of a Lagrangian trajectory $\langle\mathcal{R}(t)\rangle$ and its rms $\sigma_{\mathcal{R}}$, versus time, for two different values of σ_Y and three starting positions: $\sigma_Y = 1$-solid line, $\sigma_Y = 2$-dashed line; $(x_0, \rho_0) = (2, 0.1)$-thin curve (first particle), $(x_0, \rho_0) = (2, 0.9)$-the

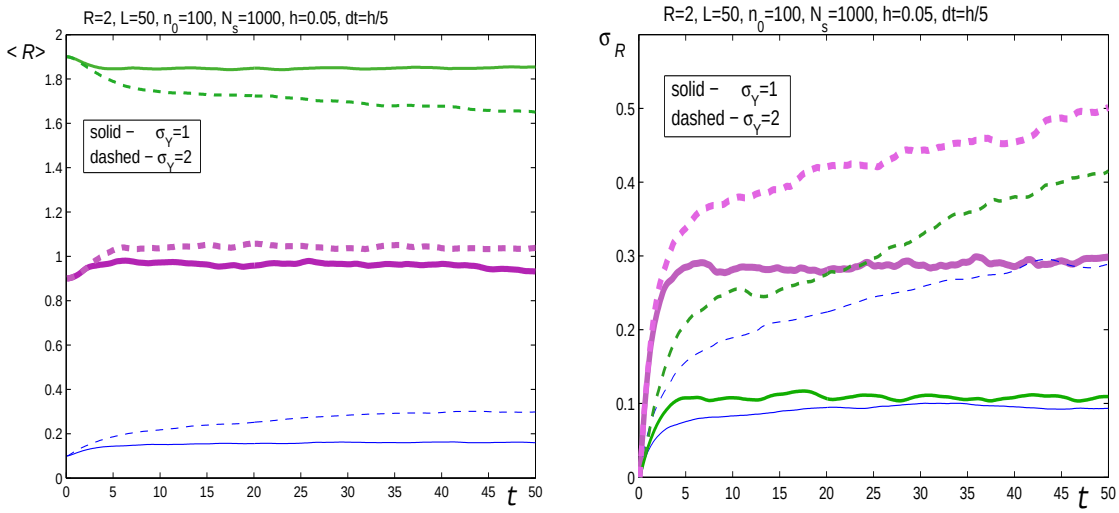

Figure 11: The mean of the transverse coordinate of a Lagrangian trajectory as a function of time, for three different starting transverse positions, for two values of σ_Y (left panel), and its standard deviation (right panel). The thin curves corresponds to the starting value $\rho_0 = 0.1$, the medium thick curves correspond to $\rho_0 = 0.9$, and the bold thick curves for $\rho_0 = 1.9$.

medium thick curve (second particle), and $(x_0, \rho_0) = (2, 1.9)$-the bold thick curve (third particle). In what follows, if otherwise not indicated, we fix $R = 2$, $L = 50$, and the sample size $N_s = 1000$. Note that the rms of the Eulerian velocity in the layer where the second particle was started is larger than that of the layers where the first and third particles were started (see Figure 3), it is to expected that the same relations hold for the rms' $\sigma_{\mathcal{R}}$ of the Lagrangian velocities. This was confirmed in simulations, see Figure 11 (right panel). Note however that the variation in time of the mean transverse coordinate $\langle \mathcal{R}(t) \rangle$ is considerably less for the second particle than for the first and third particles. This is related to the fact that the Eulerian velocity in the layers around $\rho = R/2 = 1$ is more homogeneous than that at the layers close to the boundary of the tube, i.e., at $\rho = 0$ and $\rho = R = 2$).

In Figure 12 we plot the Lagrangian statistical characteristics $\langle X(t, x_0, \rho) \rangle$ and $\langle X'^2(t, x_0, \rho) \rangle$ versus time, for the same values of σ_Y and starting points chosen in the calculations presented in Figure 11. One might expect, in analogy with the case of the transverse coordinate, that these Lagrangian characteristics will be larger for the first particle (which has started in a layer near the axis of the tube where both the mean and rms of the Eulerian velocity are larger than that of the layers closer to the boundary where the second and third particles were started, see Figure 1) than that for the second and third particles. However it is not true. In Figure 12 we see that starting from a certain time ($t \simeq 3$), the values $< X(t, x_0, \rho) >$ and $\langle X'^2(t, x_0, \rho) \rangle$ for the first particle become smaller than that of the second and third particles.

It looks like a contradictory. Indeed, both the mean longitudinal Eulerian velocity $\langle u_x \rangle$ and the r.m.s σ_u in the layers close to the axis where the first particle is mainly walking ($\rho_0 = 0.1$) are larger than those for the layers where the second and third particles are moving. But nevertheless, the mean longitudinal Lagrangian velocity of the first particle becomes rapidly smaller than the mean longitudinal Lagrangian velocities of the second and third particles.

But this is not a contradictory, and can be explained as follows.

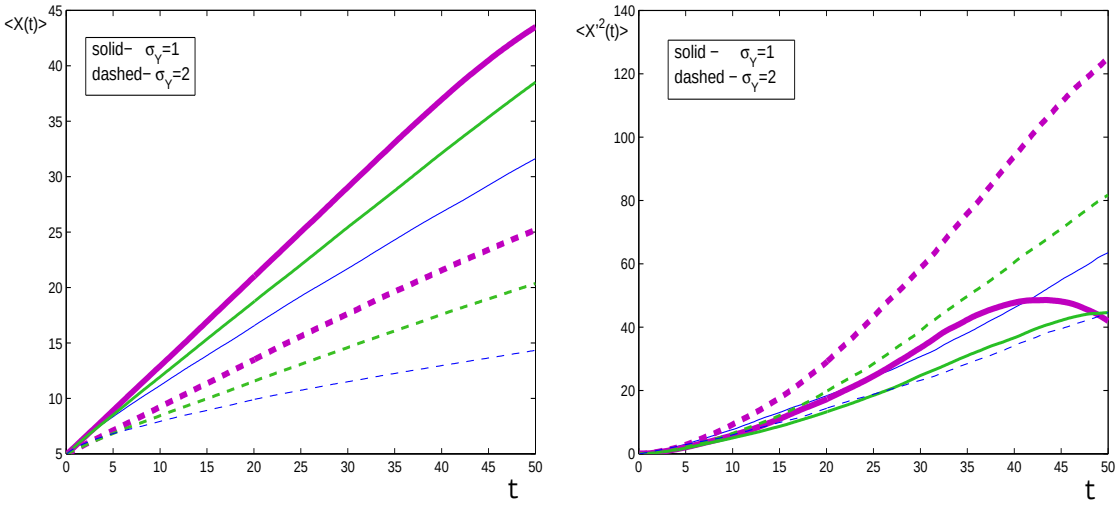

Figure 12: Mean of the longitudinal Lagrangian coordinate (left panel) and its variance (right panel), as a function of time, for two values of σ_Y, and different values of ρ_0. The thin curves corresponds to the starting value $\rho_0 = 0.1$, the medium thick curves correspond to $\rho_0 = 0.9$, and the bold thick curves present the case $\rho_0 = 1.9$.

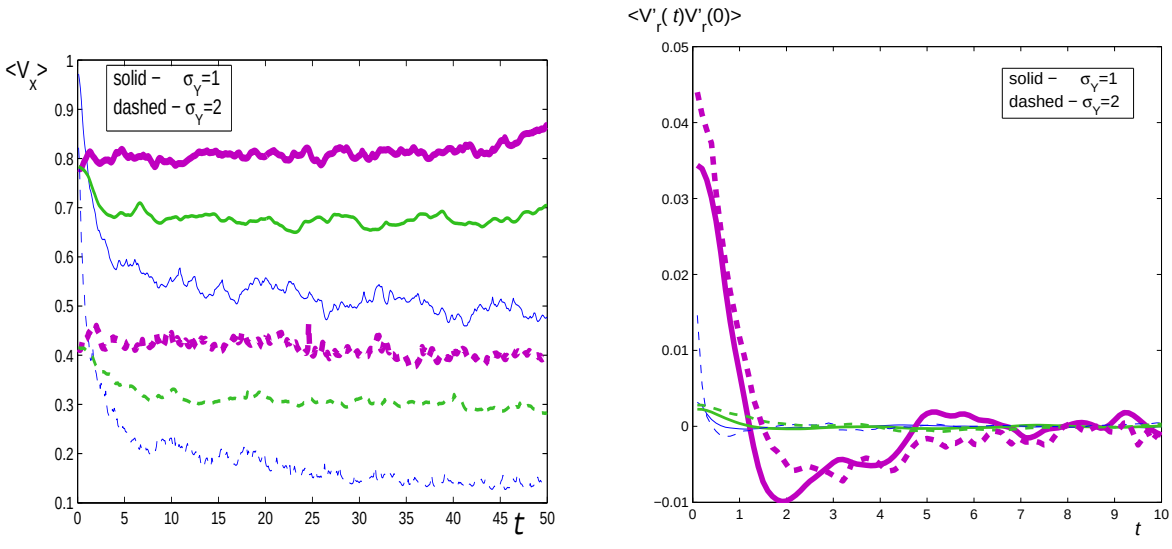

Figure 13: The mean of the transverse Lagrangian velocity (left panel), and the Lagrangian correlation function of the transverse velocity (right panel), for three different values of ρ_0, and two values of σ_Y.

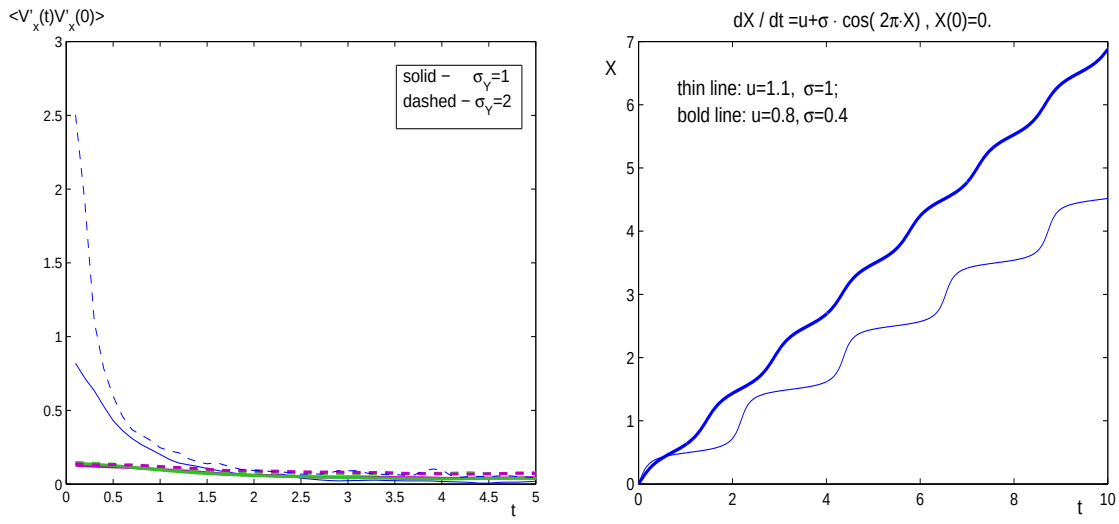

Figure 14: Left panel: Lagrangian correlation function of the longitudinal velocity as a function of time, for three different values of ρ_0, and two values of σ_Y.
Right panel: Illustration to the "stagnation" effect: having larger velocity does not imply the particle moves faster.

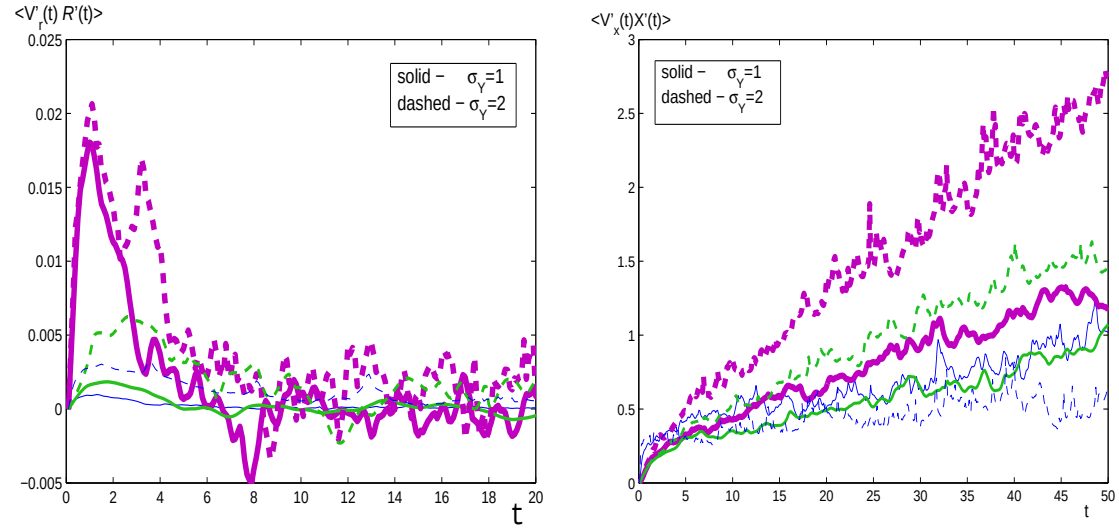

Figure 15: Transverse (left panel) and longitudinal (right panel) diffusion coefficients versus time, for three different values of ρ_0, and two values of σ_Y.

Let us consider a one-dimensional movement governed by the following equation

$$dX/dt = u + \sigma \cos(2\pi * X), \qquad X(0) = 0.$$

In Figure 14 (right panel) we show two variants of the solution to this equation corresponding to the following values of the mean (u) and variance (σ): (1) $u = 1.1, \sigma = 1$, and (2), $u = 0.8, \sigma = 0.4$. It is seen that the particle having larger values of u and σ has smaller mean displacement than that of the particle with smaller u and σ. The reason of this phenomenon is clear: the particle with a larger value of σ spends more time in regions with very small Eulerian velocities. Thus the particles with smaller value of σ are not so often trapping by this "stagnation regions", and their average movement is faster. Of course, this is only an illustrative example, but it clearly shows that the particles with larger velocity and larger variance may be more probable trapped by the stagnation regions.

Back to the Figure 12, the non-monotone behavior of $\langle X'^2(t, x_0, \rho)\rangle$ for the second particle (see Figure 12, right panel) is due to the stopping rule of our simulation algorithm: particles reaching the right end of the tube at a certain time are staying there, hence many of particles show after $t > 35$ unphysical behavior.

In Figure 13 (left panel) we present the mean longitudinal Lagrangian velocity versus time. The same as in Figure 12, the value of this velocity for the first particle is less than that of the second and third particles. In Figure 13 (right panel) and Figure 14 (left panel) we present the Lagrangian correlation functions for the transverse and longitudinal velocity components, respectively. From the results of Figure 13 (right panel) it is seen that for all the particles, the Lagrangian correlation function for the transverse velocity tends to zero as time increases, while the Lagrangian correlation function for the longitudinal velocity it is not so. This is in agreement with the relevant Eulerian statistical characteristics, see Figures 5 and 6. This may lead to a failure of the Fickian diffusion law , see the curves $\langle X'^2(t, x_0, \rho)\rangle$ in Figure 12 (right panel).

In Figure 15 we show the coefficients of the transverse and longitudinal diffusion. Notice that the transverse diffusion coefficient is first rapidly increasing in time, reaches a maximum, and then slowly decreases and fluctuates around zero. This behavior was also reported in [27].

As to the longitudinal diffusion coefficient, it monotonically increases in time. It should be noted that as σ_Y increases, the longitudinal diffusion coefficient tends to a constant asymptotics. This implies that as σ_Y increases, we may expect the Fickian law for long tubes.

There is a high both theoretical and practical interest in finding relations between Lagrangian and Eulerian statistical characteristics, in particular, the time evolution of the Lagrangian velocity pdf starting from the known Eulerian pdf at the initial time instant. In our numerical experiments we have compared $p_L(u; t) = \langle u - V_x(t)\rangle$, the pdf of the longitudinal Lagrangian velocity, for two times, $t = 0$, and $t = 13$. Note that after $t = 13$, the density $p_L(u, t)$ behaves close to a quasi-stationary regime, i.e., it weakly depends on time.

In Figures 16-18 we present the histograms for the pdf $p_L(u, t)$ at $t = 0$ (left panels) and $t = 13$ (right panels), for our three particles' starting positions, for a fixed value of dispersion, $\sigma_Y = 1$. As mentioned above, the statistics was carried out over $N_s = 1000$ samples, for the tube with $R = 2$, $L = 50$. To see a deviation from the Gaussian behavior, we plot also the Gaussian densities with the means and variances of the corresponding histograms.

From these results it is seen that only for the second particle the pdf can be approximated by a Gaussian curve for all times. It was also noticed that with the time, the right tails become weaker while the left tails' weight increases.

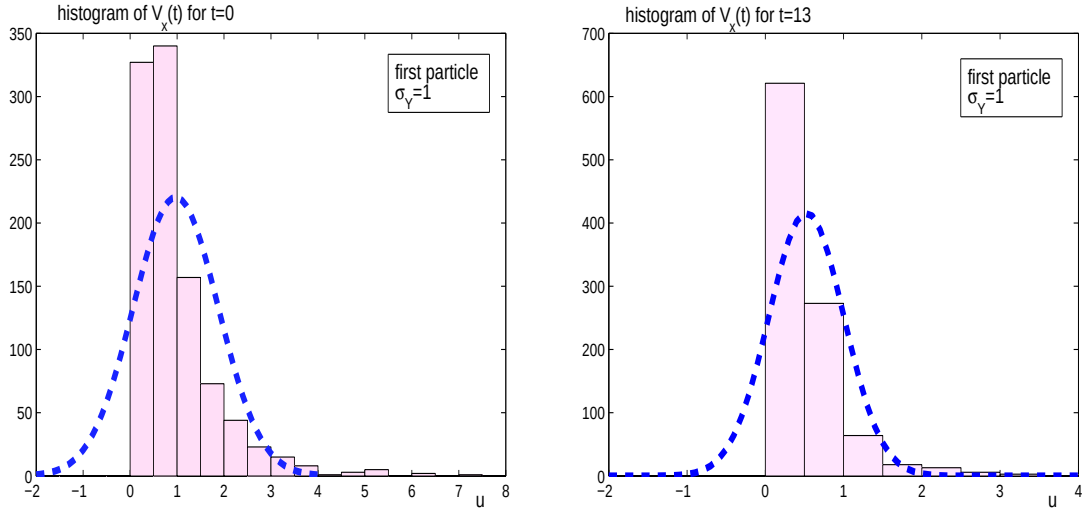

Figure 16: Histograms of the longitudinal Lagrangian velocity, for the first particle ($\rho_0 = 0.1$), at the time instants $t = 0$ (left panel), and $t = 13$ (right panel), for $\sigma_Y = 1$.

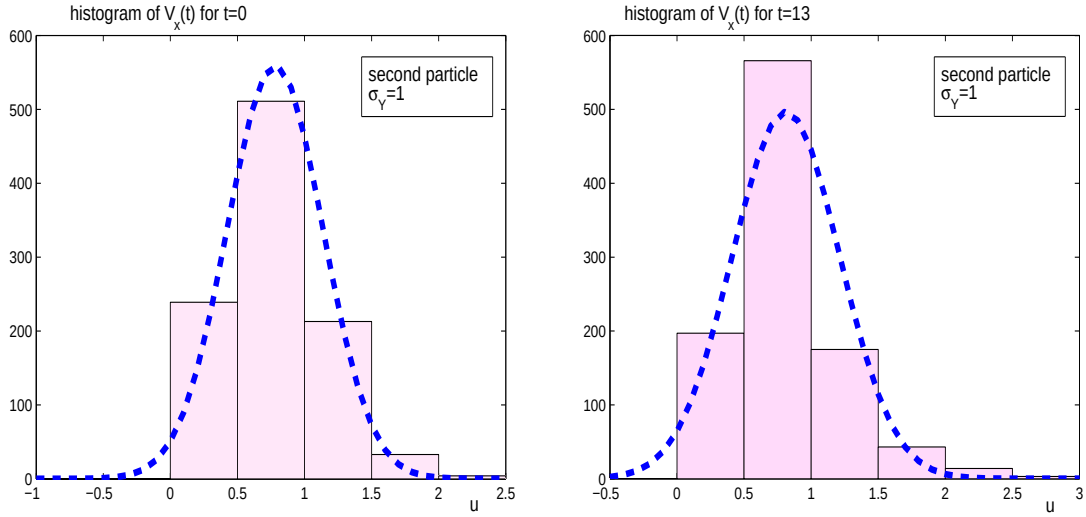

Figure 17: The same as in Figure 16, but for the second particle ($\rho_0 = 0.9$).

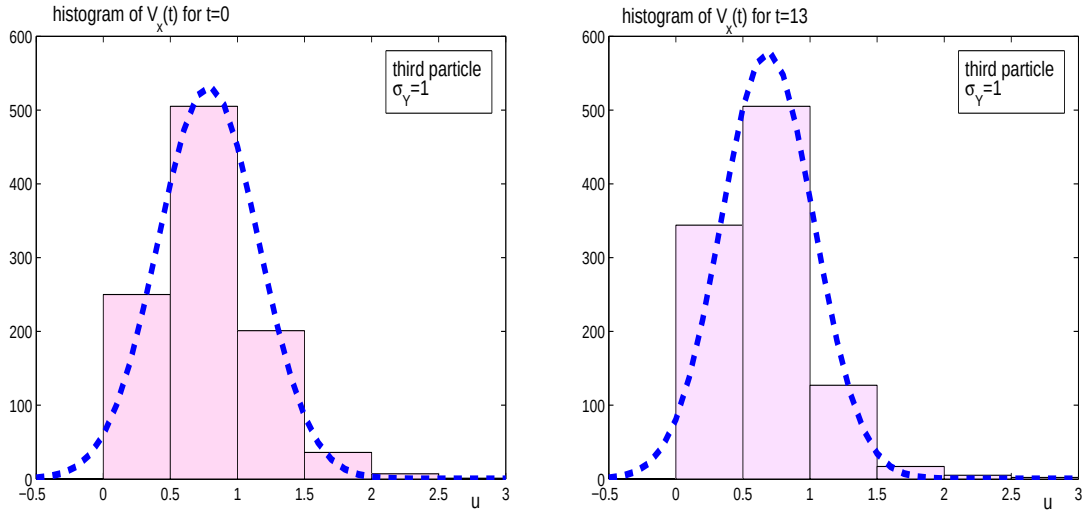

Figure 18: The same as in Figure 16, but for the third particle ($\rho_0 = 1.9$).

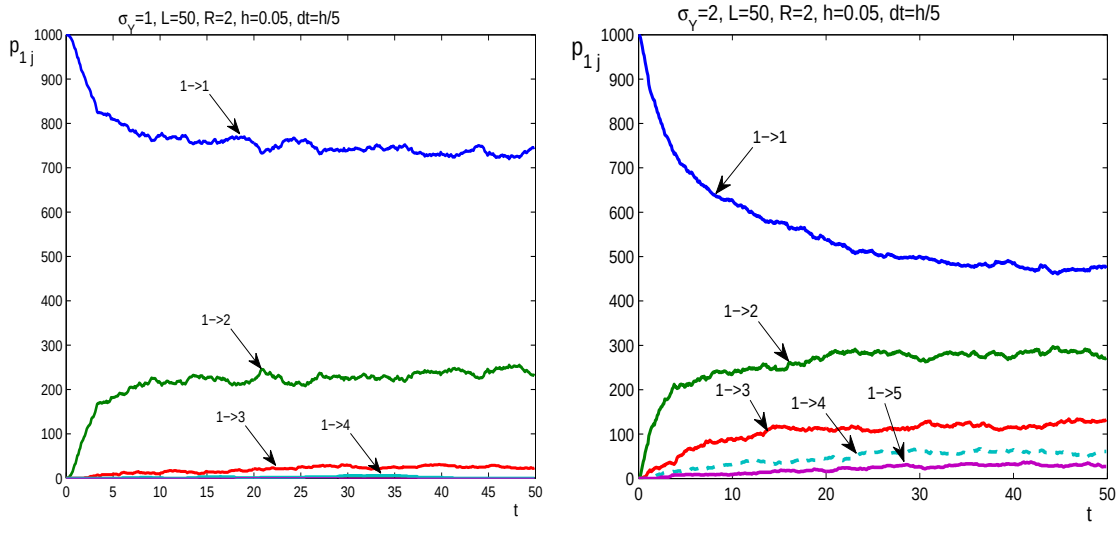

Figure 19: The time evolution of $p_{1\,j}$ for two different values of σ_Y: $\sigma_Y = 1$ (left panel), $\sigma_Y = 2$ (right panel)

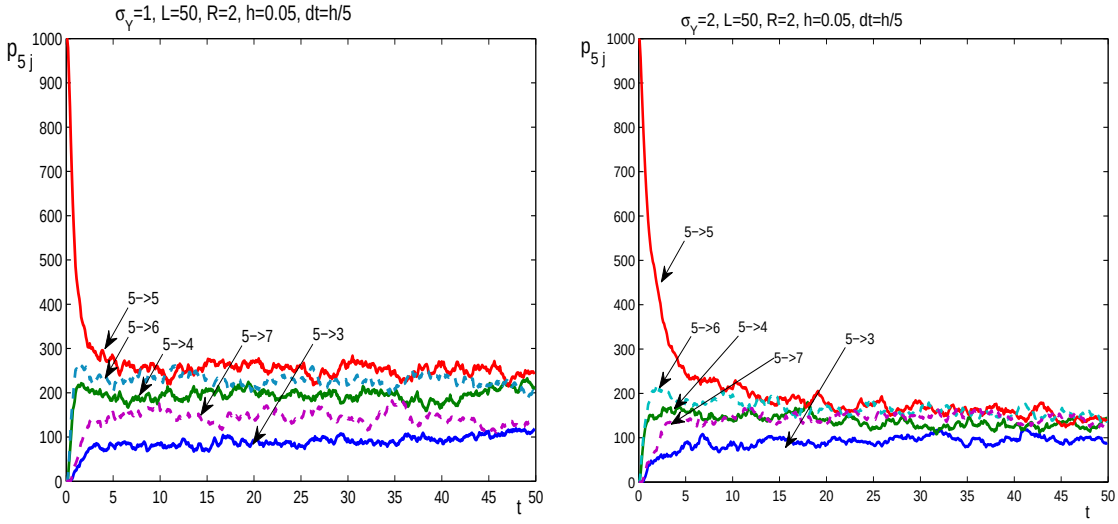

Figure 20: The same as in Figure 19 but for the fifth particle

In the sensitivity analysis it is important to relate the input characteristics, in our case say the correlation scale of the log conductivity and its rms, with the measurable quantities, like the concentration of a passive scalar from an instantaneous point source which is in the case of an incompressible flow just a transition probability density function of a Lagrangian trajectory. In our numerical experiments we have studied the transition density characterizing a transverse (radial) migration of the Lagrangian trajectories in the tube.

Let us denote by $p_{\rho_0\to\rho}(t,x_0)$ the transition density (in ρ) which is a probability density of a particle started at $t_0=0$ in a point $(x_0,\rho_0$. We are studying the situation where $p_{\rho_0\to\rho}(t,x_0)$ is weakly dependent on the starting coordinate for $x>2$. Therefore, there is no need to include x_0 in the transition density.

Thus let us denote by $p_{\rho_0\to\rho}(t)$ the transition density which is a probability density that a particle starting at the radial distance ρ_0 will have the radial coordinate ρ at the time t. To present the calculation of this function, we divide the interval $0\le\rho\le 2$ in 10 parts: $\Delta_i=[(i-1)\cdot 0.2, i\cdot 0.2]$, $i=1,...,10$, $[0,2]=\cup_{1\le i\le 10}\Delta_i$. By $p_{i\,j}(t)$ we denote the probability that a particle starting at the center of the interval Δ_i (we call it i-th particle) will appear in the interval Δ_j at the time t. For simplicity we have not normalized these probabilities on the number of tracking particles (which was $N_s=1000$), hence in Figures 19 and 20 p_{ij} is simply the number of Lagrangian particles involved in the transition $i\to j$ versus time. We show in Figure 19 the time evolution of $p_{1\,j}$ for two different values of σ_Y: $\sigma_Y=1$ (left panel), $\sigma_Y=2$ (right panel). It is seen from these results that if the changes are happened in a short time interval ($t<10$), then the curves tend to a quasi-stationary regime. In Figure 20 we show the same picture but for the fifth particle.

Let us introduce a transition probability averaged over the time interval $[t_0,t_1]$:

$$P_{i\,j}=\frac{1}{t_1-t_0}\int_{t_0}^{t_1} p_{i\,j}(t)\,dt\ .$$

We choose $t_0=15$, $t_1=35$. The choice $t_0=15$ corresponds to the time where $p_{i\,j}(t)$ begins to have a quasi-stationary behavior. The choice of $t_1=35$ is made so that for $t<t_1$, the trajectories started at $x_0=2$) do not reach the right end of the tube $x=L=50$ with high probability.

Table 1: Transition probabilities

	1	2	3	4	5	6	7	8	9	10
1	0.74	0.23	0.02	0.00	0.00	0.00	0.00	0.00	0.00	0.00
2	0.12	0.42	0.29	0.12	0.03	0.00	0.00	0.00	0.00	0.00
3	0.02	0.19	0.32	0.25	0.14	0.05	0.01	0.00	0.00	0.00
4	0.00	0.06	0.19	0.27	0.23	0.15	0.06	0.01	0.00	0.00
5	0.00	0.02	0.09	0.19	0.25	0.22	0.14	0.06	0.01	0.00
6	0.00	0.00	0.03	0.10	0.19	0.24	0.23	0.14	0.04	0.00
7	0.00	0.00	0.01	0.04	0.11	0.19	0.26	0.25	0.12	0.01
8	0. 00	0. 00	0.00	0.01	0.04	0.11	0.21	0.30	0.27	0.05
9	0. 00	0. 00	0. 00	0.00	0.00	0.03	0.09	0.24	0.41	0.22
10	0.00	0. 00	0. 00	0.00	0.00	0.00	0.00	0.03	0.20	0.76

Table 2: Transition probabilities

	1	2	3	4	5	6	7	8	9	10
1	0.48	0.28	0.12	0.06	0.03	0.01	0.00	0.00	0.00	0.00
2	0.14	0.25	0.20	0.16	0.10	0.07	0.04	0.02	0.00	0.00
3	0.07	0.13	0.19	0.17	0.15	0.11	0.08	0.04	0.02	0.01
4	0.04	0.08	0.13	0.17	0.16	0.14	0.11	0.08	0.04	0.03
5	0.03	0.05	0.09	0.13	0.16	0.15	0.14	0.11	0.06	0.04
6	0.03	0.03	0.07	0.11	0.13	0.15	0.15	0.14	0.10	0.07
7	0.02	0.02	0.04	0.07	0.11	0.14	0.16	0.16	0.14	0.11
8	0.02	0.01	0.03	0.05	0.08	0.11	0.14	0.18	0.19	0.16
9	0.02	0.01	0.01	0.03	0.04	0.08	0.12	0.17	0.24	0.27
10	0.01	0.01	0.01	0.01	0.02	0.03	0.06	0.11	0.24	0.5

In Tables 1, 2 we present the transition probabilities $P_{i\,j}$ for the same values of σ_Y which were taken in Figures 19-20: $\sigma_Y = 1$ (Table 1), and $\sigma_Y = 2$ (Table 2).

The detailed distribution shown in the Tables can be used to study the probability density function of the transverse Lagrangian coordinate,

$$p_{\mathcal{R}}(r, t; x_0,\, \rho_0) = \langle \delta(r - \mathcal{R}(t; x_0,\, \rho_0;)) \rangle.$$

Note that the incompressibility of the flow implies that after some time, say, τ_{wm}, the distribution of the transverse coordinates $X_2(t; \mathbf{x}_0)$ and $X_3(t; \mathbf{x}_0)$ will be almost uniform in the disc of radius R, i.e., the density of the transverse coordinate $\mathcal{R}(t; x_0,\, \rho_0;)$ in the cylindrical coordinates becomes linear, $p_{\mathcal{R}}(r, t; x_0,\, \rho_0) = 2r/R^2$.

For $t \geq \tau_{wm}$, the average of the longitudinal Lagrangian velocity $\bar{V}_x(t; x_0,\, \rho_0)$ will be equal to the Eulerian average U_x. Therefore, the curve $\bar{V}_x(t; x_0,\, \rho_0)$ considered as a function of t can be used to estimate τ_{wm}.

Along with τ_{wm}, there is another Lagrangian time scale, τ_L which characterizes the Lagrangian characteristic time of the transverse velocity which is defined so that for $t \geq \tau_L$, the longitudinal

dispersion $D_X(t; x_0, \rho_0)$ becomes linear in time, and hence the diffusion coefficient $K_x(t; x_0, \rho_0)$ tends to an asymptotic constant value K_∞ . These two time scales, τ_{wm} and τ_L, are practically independent of the starting coordinate (x_0, ρ_0), but they do depend on the external parameters R and σ_Y. These time scales are important which shows the following arguments. Let us introduce a length scale $x_* = U_x \max\{\tau_{wm}, \tau_L\}$. Then the mean concentration $C = \langle c \rangle$ will be governed for $x \geq x_*$ by a one-dimensional diffusion equation (3), where we should take $Q_0 = \int_{R^2} q_0(x_1, x_2) dx_1 dx_2$, $U = U_x$ and $D_m = K_\infty$.

5 Appendix: some simulation formulae

5.1 Simulation of log conductivity

Let $F(\mathbf{k})$, $\mathbf{k} \in I\!R^2$ be the spectral function of $\mathcal{Y}'$:

$$B_{\mathcal{Y}}(x, \rho) = \langle \mathcal{Y}'(x + x', \rho + \rho')\mathcal{Y}'(x', \rho') \rangle = \int_{R^2} e^{\mathrm{i}2\pi(k_1 x + k_2 \rho)} F(k_1, k_2)\, dk_1 dk_2.$$

The field $\mathcal{Y}'$ can be simulated by the randomization method:

$$\mathcal{Y}'(x, \rho) = \frac{1}{\sqrt{n_0}} \sum_{j=1}^{n_0} \left(\frac{F(\mathbf{k}_j)}{p(\mathbf{k}_j)} \right)^{1/2} \{ \xi_j \cos\theta_j + \xi'_j \sin\theta_j \}$$

where ξ_j, ξ'_j, $j = 1, ..., n_0$ are mutually independent, standard Gaussian random variables, $\mathbf{k}_j$, $j = 1, ..., n_0$ are mutually independent and independent of ξ_j, ξ'_j, $j = 1, ..., n_0$, 2D random vectors with the common pdf $p(\mathbf{k})$ (satisfying the consistency condition $p(\mathbf{k}) > 0$ if $F(\mathbf{k}) > 0$), $\theta_j = 2\pi(k_{1,j} x + k_{2,j} \rho)$.

5.2 Simulation of random fields with the Gaussian correlation function (11)

$$B_{\mathcal{Y}}(x, \rho) = \sigma^2 e^{-x^2/l_x^2 - \rho^2/l_\rho^2}, \quad F(k_1, k_2) = \sigma^2 \pi l_x l_\rho e^{-\pi^2(k_1^2 l_x^2 + k_2^2 l_\rho^2)}.$$

Take the 2D pdf

$$p(\mathbf{k}) = \pi l_x l_\rho e^{-\pi^2(k_1^2 l_x^2 + k_2^2 l_\rho^2)}.$$

Then the random vector $\mathbf{k}$ with this pdf can be simulated by the formula $\mathbf{k} = \frac{1}{\sqrt{2}\pi}(\eta/l_x, \eta'/l_\rho)$ where η, η' are independent standard Gaussian random variables. Therefore,

$$\mathcal{Y}'(x, \rho) = \frac{\sigma}{\sqrt{n_0}} \sum_{j=1}^{n_0} (\xi_j \cos\tilde{\theta}_j + \xi'_j \sin\tilde{\theta}_j) \tag{27}$$

where $\tilde{\theta}_j = \sqrt{2}(\eta_j x/l_x + \eta'_j \rho/l_\rho)$, and ξ_j, ξ'_j, η_j, η'_j, $(j = 1, ..., n_0)$ are mutually independent standard Gaussian random variables.

5.3 Simulation of random fields with the exponential correlation function (12)

The correlation function

$$B_{\mathcal{Y}}(x, \rho) = \sigma_Y^2 e^{-(x^2/l_x^2 + \rho^2/l_\rho^2)^{1/2}}$$

has the spectral function

$$F(k_1,k_2) = 2\pi l_x l_\rho \sigma_Y^2 \left(1 + (2\pi k_1 l_x)^2 + (2\pi k_2 l_\rho)^2\right)^{-3/2}.$$

If we take

$$p(\mathbf{k}) = 2\pi l_x l_\rho \left(1 + (2\pi k_1 l_x)^2 + (2\pi k_2 l_\rho)^2\right)^{-3/2} \ ,$$

then the simulation formula for $\mathbf{k} = (k_1, k_2)$ with this probability density function is $k_1 = (1/\gamma_2^2 - 1)\cos(2\pi\gamma_1)/(2\pi l_x)$, $k_2 = (1/\gamma_2^2 - 1)\sin(2\pi\gamma_1)/(2\pi l_\rho)$, where γ_1, γ_2 are two independent random variables uniformly distributed in $[0,1]$. Therefore, the random field $\mathcal{Y}$ with the exponential correlation function (12) can be simulated by the formula (27) where ξ_j and ξ'_j, $j = 1, ..., n_0$ are mutually independent standard Gaussian random variables; $\tilde{\theta}_j = (1/\gamma_{2,j}^2 - 1)[\cos(2\pi\gamma_{1,j})\, x/l_x + \sin(2\pi\gamma_{1,j})\, \rho/l_\rho]$, and $\gamma_{1,j}$, $\gamma_{2,j}$, $j = 1, ..., n_0$ are mutually independent and independent of ξ_j and ξ'_j, $j = 1, ..., n_0$ random variables uniformly distributed in $[0,1]$.

Remark 2. Let us recall that in the literature, one uses different definitions of the Fourier transform which leads also to different definitions of the spectral tensors. We give here the relation between the two different definitions, namely,

$$F_{ij}(\mathbf{k}) = \int\limits_{R^d} e^{-\mathrm{i}\,2\pi\,\mathbf{k}\cdot\mathbf{r}} B_{ij}(\mathbf{r})\, d\mathbf{r}, \quad \text{with} \quad B_{ij}(\mathbf{r}) = \int\limits_{R^d} e^{\mathrm{i}\,2\pi\,\mathbf{r}\cdot\mathbf{k}} F_{ij}(\mathbf{k})\, d\mathbf{k}, \tag{28}$$

and

$$F'_{ij}(\mathbf{k}) = \frac{1}{(2\pi)^d} \int\limits_{R^d} e^{-\mathrm{i}\,\mathbf{k}\cdot\mathbf{r}} B_{ij}(\mathbf{r})\, d\mathbf{r}, \quad \text{with} \quad B_{ij}(\mathbf{r}) = \int\limits_{R^d} e^{\mathrm{i}\,\mathbf{r}\cdot\mathbf{k}} F'_{ij}(\mathbf{k})\, d\mathbf{k}\ . \tag{29}$$

It follows from these definitions that

$$F(\mathbf{k}) = (2\pi)^d\, F'(2\pi\,\mathbf{k}), \quad \text{and} \quad F'(\mathbf{k}) = \frac{1}{(2\pi)^d}\, F(\frac{\mathbf{k}}{2\pi}).$$

For example, let us consider the correlation function $B(\rho) = e^{-|\rho|}$, $\rho \in I\!R^1$. In this case, $F(k) = \frac{2}{1+(2\pi k)^2}$, and $F'(k) = \frac{1}{\pi(1+k^2)}$.

6 Conclusion

We have developed a Monte Carlo method for stochastic simulation of flows and particle transport in tubes filled with a porous medium. The porous medium is characterized by a hydraulic conductivity which is assumed to be a lognormal random field with a Gaussian correlation function. A crucial role plays a multiscale randomization spectral method for simulation of fractal random fields developed in a recent author's paper. Numerical experiments are carried out by solving the random Darcy equation for each sample of the hydraulic conductivity by a SOR iteration method, and tracking Lagrangian trajectories in the simulated flow.

We present a numerical analysis of different Eulerian and Lagrangian statistical characteristics of the flow such as transverse and longitudinal velocity correlation functions, diffusion coefficients, the mean and variance of Lagrangian trajectories, and probability density function of the Lagrangian velocities. We give an explanation of a "stagnation" effect which was found in our simulations. The next step in these studies on the extension of the model to a full 3D case will be shown in a forthcoming publication.

References

[1] Rachid Ababou, Dennis McLaughlin, Lynn W. Gelhar and Andrew F.B. Tompson. Numerical simulation of three-dimensional saturated flow in randomly heterogeneous porous media. Transport in Porous Media, **4** (1989), N 6, 549-565.

[2] G. Dagan. Flow and Transport in Porous Formations. Springer-Verlag, Berlin-Heidelberg, Germany, 1989.

[3] G. Dagan. Spatial moments, Ergodicity, and Effective Dispersion. *Water Resour. Res.,* **26**, No. 6, 1990, 1281-1290.

[4] G. Deodatis and M. Shinozuka. Simulation of stochastic processes by spectral representation. Applied Mechanics Reviews, **44**, No.4, 1991, 191-204.

[5] Jean-Raynald Dreuzy, Anthony Beaudoin, and Jocelyne Erhel. Asymptotic dispersion in 2D heterogeneous porous media determined by parallel numerical simulations. *Water Resour. Res.*, **43** (2007), W10439.

[6] Freeze R.A. A stochastic-conceptual analysis in groundwater flow in non-uniform, homogeneous media. Water Resour. Res., **11** (1975), N 5, 725-741.

[7] J. C. H. Fung, J. C. R. Hunt, N. A. Malik, and R. J. Perkins. Kinematic simulation of homogenous turbulence by unsteady random Fourier modes. *J. Fluid Mech.*, 236:281–318, 1992.

[8] Lynn W. Gelhar. *Stochastic Subsurface Hydrology.* Prentice-Hall, Englewood Cliffs, N.J., 1993.

[9] Roger G. Ghanem, Pol D. Spanos. Stochastic finite elements. A spectral approach. Courier Dover Publications, 2003.

[10] Gikhman I.I. and Skorohod A.V. *Introduction to the Theory of Random Processes.* Philadelphia, W.B., Sounders Company, 1969.

[11] A.E. Hassan, J.H. Cushman, J.W. Delleur. A Monte Carlo assessment of Eulerian flow and transport perturbation models. *Water Resour. Res.*, **34**, 1143-1163, 1998.

[12] D. Kolyukhin and K. Sabelfeld. Stochastic flow simulation in 3D Porous media. *Monte Carlo Methods and Applications*, **11**, No. 1, 2005, 15-37.

[13] R.H. Kraichnan. Diffusion by a random velocity field. Phys.Fluids, **13** (1970), N1, 22-31.

[14] P. Kramer, O. Kurbanmuradov, and K. Sabelfeld. Comparative Analysis of Multiscale Gaussian Random Field Simulation Algorithms. Journal of Computational Physics, v. 226 (2007), 897-924.

[15] O. Kurbanmuradov, K. Sabelfeld, and D. Koluhin. Stochastic Lagrangian models for two-particle motion in turbulent flows. Numerical results. *Monte Carlo Methods Appl.*, 3(3):199–223, 1997.

[16] Kurbanmuradov O., Sabelfeld K., Smidts O. and Vereecken H.A. Lagrangian stochastic model for transport in statistically homogeneous porous media. *Monte Carlo Methods and Applications.* **9**, No. 4, 2003, 341-366.

[17] Kurbanmuradov O. and Sabelfeld K.K. Stochastic spectral and Fourier-wavelet methods for vector Gaussian random field. Monte Carlo Methods and Applications, vol.12, N 5-6.

[18] Mikhailov G.A. Approximate models of random processes and fields. Russian J. Comp. Mathem. and mathem. Physics, vol.23 (1983), N3, 558-566. (in Russian).

[19] A.S. Monin and A.M. Yaglom. *Statistical Fluid Mechanics: Mechanics of Turbulence*, Volume 2. The M.I.T. Press, 1981.

[20] Sabelfeld, K.K. *Monte Carlo Methods in Boundary Value Problems.* Springer-Verlag, Berlin – Heidelberg – New York, 1991.

[21] Sabelfeld K. and Kolyukhin D. Stochastic Eulerian model for the flow simulation in porous media. Monte Carlo Methods and Applications. vol.9, N3, 271-290, 2003.

[22] Salandin, P., and V. Fiorotto. Solute transport in highly heterogeneous aquifers. Water Resour. Res., **34**, 949-961.

[23] A.A. Samarskii, E.S. Nikolaev. Numerical Methods for Grid Equations, Birkhauser, 1989

[24] H. Schwarze, U. Jaekel and H. Vereecken. Estimation of Macrodispersion by Different Approximation Methods for Flow and Transport in Randomly Heterogeneous Media. *Transport in Porous Media*, **49**(2001), 2, 267-287.

[25] M. Shinozuka. Simulation of multivariate and multidimensional random processes. J. of Acoust. Soc. Am. **49** (1971), 357-368.

[26] L. Smith and R.A. Freeze. Stochastic Analysis of Steady State Groundwater Flow in a Bounded Domain, 2. Two-Dimensional Simulation. *Water Resour. Res.*, **15**(6), 1543-1559, 1979.

[27] Suciu N., C. Vamos, K. Sabelfeld, and. C. Andronache (2007). Memory effects and ergodicity for diffusion in spatially correlated velocity fields, Proc. Appl. Math. Mech., 7, 2010015-2010016, doi:10.1002/pamm.20070057.

[28] Tompson, A.F.B., and L.W. Gelhar. Numerical simulation of solute transport in tree-dimensional randomly heterogeneous porous media. *Water Resour. Res.*, **26**(10), 2541-2562, 1990.

[29] D. J. Thomson and B.J. Devenish. Particle pair in kinematic simulations. *Journal of Fluid Mechanics*, **526** (2005), 277-302.

[30] Jichun Wu, Bill X. Hu, Dongxiao Zhang and Craig Shirley. A three-dimensional numerical method of moments for groundwater flow and solute transport in a nonstationary conductivity field Advances in Water Resources, **26** (2003), N 11, 1149-1169.

[31] A. M. Yaglom. *Correlation theory of stationary and related random functions. Volume I: Basic results.* Springer-Verlag, Berlin, 1987.

[32] J. Yang, D. Zhang, Z. Lu. Stochastic analysis of sturated-unsaturated flow in heterogeneous media by combining Karhunen-Loeve expansion and perturbation method. Journal of Hydrology. 294(2004) 18-38.

[33] L. A. Hageman. and D. M. Young. Applied Iterative Methods. Academic Press, New York, 1981.

[34] Dongxiao Zhang and Zhiming Lu. An efficient, high-order perturbation approach for flow in random porous media via Karhunen-Loeve and polynomial expansions. *Journal of Comp. Physics*, **194**, 773-794, 2004.

[35] Dongxiao Zhang. Stochastic Methods for Flow in Porous Media. Coping with Uncertainties. Academic press, 2001,